Approach to coherent interference fringes in helium-surface scattering

Matthew C. Schram*
Department of Physics, Massachusetts Institute of Technology, Cambridge, Massachusetts 02139, USA

Eric J. Heller†
Department of Physics, Harvard University, Cambridge, Massachusetts 02138, USA

(Received 24 March 2018; published 28 August 2018)

The conventional notion of elastic, coherent atom-surface scattering originates from the scattering particles acting as a quantum-mechanical matter wave, which coherently interfere to produce distinct Bragg peaks which persist at finite temperature. If we introduce inelastic scattering to this scenario, the result is that the surface particles become displaced by the scattering atoms, resulting in emission or absorption of phonons that shift the final energy and momentum of the scatterer. As the lowest-lying phonons are gapless excitations, the ability to measure these phonons is very difficult and this difficulty is exacerbated by the roughly 1-eV resolution found in high-energy helium scattering experiments. Even though the surface has in effect measured the presence of the scatterer which decoheres the particle, we retain the diffraction spots which are referred to as coherent scattering. How do we reconcile these disparate viewpoints? We propose an experiment to more precisely examine the question of coherence in atom-surface scattering. We begin with an initially coherent superposition of helium particles with equal probabilities of interacting with the surface or not interacting with the surface. The beams are directed so that after the scattering event, the atoms are recombined so that we can observe the resulting interference pattern. The degree to which phonons are excited in the lattice by the scattering process dictates the fringe contrast of the interference pattern of the resulting beams. We use semiclassical techniques to simulate and test the viability of this experiment and show that for a wide range of conditions, despite the massive change in the momentum perpendicular to the surface, we can still expect to have coherent (in the superposition sense) scattering.

DOI: 10.1103/PhysRevA.98.022137

I. INTRODUCTION

Helium scattering is a valuable nondestructive experimental probe that has been useful for characterizing surface structure [1–4], measuring surface phonons [5,6], detecting surface impurities [7], and elucidating surface chemical dynamics. Over the past decade, the field has been reinvigorated due to newer, higher-energy helium sources that have allowed observation of diffraction peaks [8] from both insulator [9] (e.g., lithium fluoride) and metallic [10] (e.g., silver) surfaces. In the literature, the phrase coherent scattering has been attached to this process and strides have been made in understanding the different regimes of scattering [11] and the specifics of the outgoing diffraction pattern [12]. Seifert *et al.* [13] alluded to the notion of a Feynman-style [14] which-way measurement process caused by the scatterer-surface interaction, which we explore in more detail here in a gedanken experiment to clarify the notion of coherence (or loss thereof due to surface lattice excitations) in atom-surface scattering.

The conventional notion of coherent atom-surface scattering originates from experiments demonstrating nominally elastic Bragg peaks. The scatterer, in truly elastic scattering, acts as a quantum mechanical matter wave; it is infinite in spatial extent and is coherent with itself (represented as the wave function $\psi \propto e^{i\vec{k}\cdot\vec{r}}$). The scatterer does not in fact measure a single particle on the surface, but instead experiences the translational symmetry and maintains its inner phase coherence as it diffracts from all the lattice sites collectively and simultaneously. The outgoing waves constructively interfere and scatter into new directions $\vec{k} \rightarrow \vec{k} + \vec{G}$, where the $\{\vec{G}\}$ are the reciprocal lattice vectors of the surface. For a purely elastic process, the so-called crystal momentum is hence conserved as is the scatterer energy. Moreover, we still observe diffraction peaks when scattering off a lattice at finite temperature. While the surface atoms are at any instant displaced from their equilibrium positions (effectively eliminating the constructive interference condition at any instant), the mean atomic positions are still at the sites indexed by the crystal lattice. We thus still observe diffraction spots, although they are diminished by either an effective Debye-Waller term or another factor depending on the scattering conditions [15,16]. The description of scattering remains coherent.

However, we must include the effect of inelastic scattering. The surface particles are displaced by the scattering atom itself and may emit or absorb one or more quanta of vibrational excitations (phonons) to the scatterer. This effect occurs regardless of whether the lattice is at finite temperature or not (although the ratio of emission and absorption of phonons changes with temperature). Acoustic phonons produced by this process are gapless excitations; hence, extremely long-wavelength

*schram@mit.edu
†heller@physics.harvard.edu

phonons will contribute vanishingly small shifts in energy and momentum, making it increasingly difficult to actually observe their influence. These aspects have been studied with great success in neutron-bulk scattering [17]; however, the fundamentally different nature of the atom-surface interaction (long ranged and gradual over many sites vs short ranged and impulsive) and the challenge of generating monoenergetic atomic beams may mask this detection in atom-surface scattering. This difficulty is exacerbated by the resolution limits of the helium scattering experiment; the highest-energy phonon in lithium fluoride is approximately 80 meV [18], while the energy spread in high-energy helium scattering experiments is on the order of 10 eV for a 1-keV beam. The ability of the surface to measure the particle's presence via phonon excitation acts to destroy quantum coherence, though we still observe finite-width diffraction spots which had been taken to imply phase coherent scattering. In another work by Siefert and Winter [19], the phrase "Young-type interference" was used to denote the helium beam's self-coherence throughout the scattering process along the rows of adsorbed oxygen atoms on a Mo⟨112⟩ surface; however, the notion from a quantum measurement perspective of Young interference is a result of avoiding any emission or absorption of particles which would act to characterize which path the particle had taken. How can we reconcile these disparate perspectives?

We propose a way of looking at the question of coherence in atom-surface scattering. Instead of a single beam of helium particles, we are motivated by coherent atomic interferometric measurements [20] and start with a beam splitter to create an initially coherent superposition with equal probabilities of interacting with the surface or not interacting with the surface. The atoms then propagate along both paths simultaneously, both scattering and not scattering at the same time in the quantum mechanical sense, and then are recombined. In the case where the scattering is perfectly elastic, the two beams will have wavelike interference patterns with perfectly well-defined interference fringes. In the case of perfectly inelastic scattering, the phonon generation acts to measure the particle; we have performed a which-way measurement and we will observe no interference pattern. For partial inelasticity, we will observe behavior between these two regimes; while there will be an interference pattern, it will no longer have perfect contrast but instead have weakened fringes atop a broad background which reveals the degree of scattering inelasticity. The experiment we propose is analogous to placing a light source behind the wall of the double-slit experiment in order to test which slit the electron emerged from. The degree of lattice excitation in different scattering conditions is analogous to the strength (and hence measurement capability) of the light source.

II. MEANING OF COHERENCE

A. Self-coherence

To make this distinction and the notion of coherence more explicit, let us consider the schematic of the scattering process in the preceding experiments. If we treat the incident beam as a plane wave of wave vector $\vec{k} = (\vec{K}, k_z)$, the total wave function representing a helium atom elastically scattering off

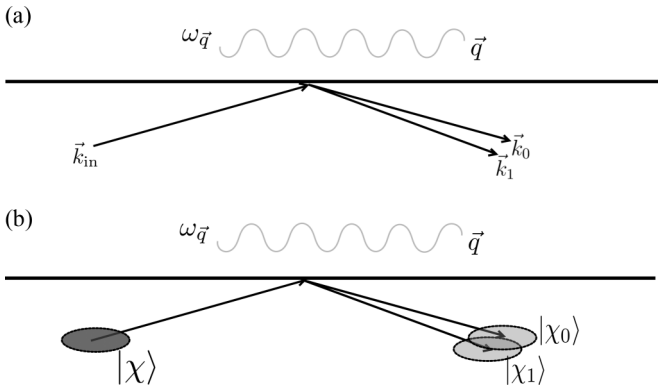

FIG. 1. Regimes of partially inelastic scattering (a) wave-vector scattering and (b) wave-packet scattering.

of a crystal surface can be expressed as

$$\psi(x, y, z) = \exp(i\vec{K}\cdot\vec{R} + ik_z z) + \sum_{\vec{G}} c_{\vec{G}} \exp[i(\vec{K}+\vec{G})\cdot\vec{R} - ik_{z_{\vec{G}}} z],$$

where $\vec{R} = (x, y)$ and the $\{\vec{G}\}$ are the reciprocal lattice vectors of the surface and $k_{z_{\vec{G}}}$ is chosen to conserve energy and momentum. This expresses the fact that at the surface the beam is coherent with itself, and the resulting emitted wave from each atom (in the Kirchhoff sense [21]) is a spherical wave; far from the surface we have the constructive interference condition $\vec{a}_i \cdot \vec{G} = 2\pi n$ with $n \in \mathbb{Z}$, i.e., crystal momentum conservation. For elastic collisions, we further have the energy conservation condition

$$\vec{k}^2 = (\vec{k}' + \vec{G})^2.$$

The conventional way of introducing inelastic scattering is to simply examine the consequence of the generation or absorption of a phonon (of momentum $\vec{q}$ and frequency $\omega_{\vec{q}}$) on the helium particle as the wave vector goes from $\vec{k}$ to $\vec{k}'$. In this case, for a surface phonon, the crystal momentum conservation condition becomes

$$\vec{K} = \vec{K}' + \vec{G} + \vec{q},$$

with energy conservation condition

$$\vec{k}^{\,2} = (\vec{k}' + \vec{G})^2 + \omega_{\vec{q}}.$$

Studies by Benedek and Toennies [6] and others have demonstrated the use of time-of-flight spectroscopy to measure surface phonon modes as a method of characterizing surface structure.

However, the above treatment does not consider the full quantum mechanical effect of including the lattice as part of the dynamics. Moreover, the phrase "coherent scattering" belies a notion of quantum mechanical coherence that cannot be justified in the sense of the absence of measurement capability of a system. Consider a hypothetical scattering event as depicted in Fig. 1(a). The helium atom scatters off an initially ground-state lattice where one single quantum of one single-phonon mode (regardless of $\vec{q}$ or $\omega_{\vec{q}}$) becomes excited with probability $|c_1|^2$. We may then write the total wave function of the outgoing

system as

$$|\Psi_{\rm out}\rangle = c_0|\vec{k}_0\rangle|\emptyset\rangle + c_1|\vec{k}_1\rangle|1\rangle. \quad (1)$$

Looking at the density matrix of the combined system yields

$$|\Psi_{\rm out}\rangle\langle\Psi_{\rm out}| = |c_0|^2[|\vec{k}_0\rangle|\emptyset\rangle\langle\emptyset|\langle\vec{k}_0|] + |c_1|^2[|\vec{k}_1\rangle|1\rangle\langle 1|\langle\vec{k}_1|] + c_0c_1^*[|\vec{k}_0\rangle|\emptyset\rangle\langle 1|\langle\vec{k}_1|] + c_0^*c_1[|\vec{k}_1\rangle|1\rangle\langle\emptyset|\langle\vec{k}_0|].$$

Using the orthogonality of wave vectors $\langle\vec{k}_0|\vec{k}_1\rangle = \delta(\vec{k}_0 - \vec{k}_1)$ and the orthogonality of the phonon modes $\langle n|m\rangle = \delta_{nm}$, we may compute the purity $\eta = {\rm Tr}[\rho_{\rm red}^2]$ [22], the quantity frequently used in the literature on decoherence phenomena in quantum mechanics to denote the coherence remaining in the system. Performing this calculation, we obtain

$$\eta_{\vec{k}} = |c_0|^4 + |c_1|^4,$$

which yields an extremely rapid decrease in the coherence of the final wave packet; in essence, a small purity value gives a sense of the magnitude of the off-diagonal elements of the bath. The possibility of exciting more quanta of other modes causes a further reduction in the purity; this is intuitive as exciting a single phonon acts to measure that the helium atom did in fact impact the surface. This is independent of phonon frequency and wave vector; as acoustic excitations are gapless excitations, there could indeed be many excitations of practically zero-frequency and zero-momentum phonons. Within this scheme, how can there possibly then be any coherent scattering if there are these types of inelastic excitations destroying the coherence of the incident wave packet?

While the idea of measurement coherence is lost, the possibility of generating finite width diffraction peaks is rescued by the fact that the incoming helium atoms are not strictly a plane wave but instead a coherent superposition of energies and momenta; the helium atoms can be considered a wave packet in momentum space (and effectively in position space as well). We might recall the requirement that x-ray scattering has either a continuum of energies or other conditions that ease the $\delta(\vec{k}_0 - \vec{k}_1)$ limit for coherent scattering to take place; similarly, the finite spread in wave-packet energy actually acts to increase the coherence of the scattered atomic beam. Consider Eq. (1) and replace the plane-wave states with a generic wave packet (considered in either momentum or position space or both) $|\chi_i\rangle$, given by

$$|\chi_0\rangle = \sum_{\vec{k}} a(\vec{k})|\vec{k}\rangle,$$

so that the full postscattering wave function becomes [as depicted in Fig. 1(b)]

$$|\Psi_{\rm out}\rangle = c_0|\chi_0\rangle|\emptyset\rangle + c_1|\chi_1\rangle|1\rangle, \quad (2)$$

where the state $|\chi_1\rangle$ captures all the distortion of the wave packet as a consequence of the scattering process. If we again calculate the purity, we obtain

$$\eta_\chi = |c_0|^4 + |c_1|^4 + 2|c_0|^2|c_1|^2|\langle\chi_0|\chi_1\rangle|^2 \geqslant \eta_{\vec{k}},$$

which will in general be much closer to unity. Moreover, in the limit that $|\langle\chi_0|\chi_1\rangle|^2 \to 1$, we have $\eta_\chi \to 1$. Looking at the distortion in the wave packet after phonon excitation yields

$$\langle\chi_0|\chi_1\rangle = \sum_{\vec{k}} a^*(\vec{k})b(\vec{k} + \vec{q}), \quad (3)$$

where $b(\vec{k})$ represents the final wave-packet momentum spread. It is clear that if the momentum-space width of the wave packet is greater than the $\vec{q}$ excitation, there may very well be (although not necessarily need to be) a vanishingly small decrease in the purity (and hence coherence) of the outgoing wave packet. The experiment by Bundaleski *et al.* [10] used a beam with a full width at half maximum energy resolution of 5 eV for a 1-keV beam; even if we include the possibility of electronic excitations, if we assume the initial momentum distribution $a(\vec{k})$ of the wave packet is Gaussian and $a(\vec{k}) = b(\vec{k} - \vec{q})$, we obtain, by integrating over Eq. (3), a possible overlap as large as ∼0.95.

Even if we consider a pure plane wave, we may still get diffraction spots from inelastic scattering, though they will be broadened. To cast the previous discussion in a more physically intuitive picture, if the scatterer disturbs the lattice to produce a phonon of wavelength λ, the Kirchhoff sum of emitted waves will produce an outgoing beam pattern with elastic diffraction peaks corresponding to the static interaction, plus a contribution to each peak of a momentum $k \sim \frac{\pi}{\lambda}$ to a phonon depending on the strength of the interaction. Roncin and Debiossac [23] describe a complementary picture to the decoherence scheme we have discussed; they note that the scattering atom acts to measure the surface atoms and induces decoherence via either position measurement (local measurements of thermal motion that is the traditional source of the Debye-Waller factor in diffraction) or momentum transfer (analogous to the surface particles undergoing emission with recoil). Toennies and co-workers [24,25] postanalyzed the scattered beam for specific energy loss, recovering Bragg peak coherence and measuring properties of surface phonons. However, when other modes with random phases are included in this sum, the scattering yields broadened diffraction peaks. If the width of the Bragg peaks produced is substantially smaller than the momentum precision of the measurement apparatus, this will be experimentally indistinguishable from perfectly elastic scattering. In this way Bragg peaks, already broadened by experimental factors like momentum dispersion in the incident beam, may mask detection of phonon production by the effect of the peak widths as outlined above.

B. Superposition coherence

Suppose that we instead took our starting beam of helium particles and sent them through a beam splitter to obtain a coherent superposition in both a left path that will undergo the scattering process and a right path absent of any coupling to the lattice degrees of freedom. The full initial wave function then becomes

$$|\psi_I\rangle = \frac{1}{\sqrt{2}}[|\vec{k}_{i\rm L}\rangle_{\rm sys} + |\vec{k}_{i\rm R}\rangle_{\rm sys}]|\{\emptyset\}\rangle_{\rm bath},$$

where we take for purposes of discussion the initial lattice state to be the ground state. Now suppose that the left wave will experience the same interaction process as in Eq. (2), exciting

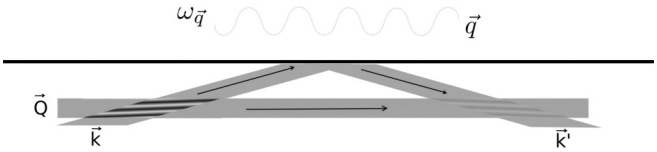

FIG. 2. Recombined scattered beam interference pattern.

one single phonon. The full final wave function becomes

$$|\psi_F\rangle = \frac{1}{\sqrt{2}}[c_0|\vec{k}_{f\mathrm{L}}\rangle_{\mathrm{sys}}|\{\emptyset\}\rangle_{\mathrm{bath}} + c_1|\vec{k}'_{f\mathrm{L}}\rangle_{\mathrm{sys}}|\{1\}\rangle_{\mathrm{bath}} + e^{i\eta}|\vec{k}_{f\mathrm{R}}\rangle_{\mathrm{sys}}|\{\emptyset\}\rangle_{\mathrm{bath}}],$$

where η is a relative path-dependent phase difference accumulated between the two beams; this process is schematically depicted in Fig. 2. Note again that this is completely independent of what the final lattice excitation was or what its length and energy scale are. When a detector or some other process measures the position of the scattered beam, we again trace (average) out the lattice coordinate, using the orthogonality of the phonon mode states. This yields the probability distribution

$$\rho_{\mathrm{red}}(\vec{r},\vec{r}\,) = \langle\vec{r}\,|\mathrm{Tr}_{\mathrm{bath}}[|\psi_F\rangle\langle\psi_F|]|\vec{r}\,\rangle = 1 + |c_0|\cos[(\vec{k}_{f\mathrm{L}} - \vec{k}_{f\mathrm{R}})\cdot\vec{r}\,]. \quad (4)$$

This provides a very clear picture; the degree to which the lattice has been excited from the ground state by the scattering process ($|c_0|$) directly determines the degree to which the particle has been measured by the lattice, and reduces the fringe contrast between the two outgoing quantum matter waves. These notions can be extended to wave packets and their respective Fourier-transformed energy eigenstates. The degree of energy loss, or stopping power, the helium particle has experienced is not directly related to $|c_0|$; while high stopping power implies small $|c_0|$, the converse is not true. This formalism leads to an interpretation of the strength of this measurement process and can be extended to any number of quanta of any number of phonon modes or any other type of excitation. This is the actual notion of coherence that we seek to understand in this work.

C. Vibrational versus electronic excitation

This work focuses primarily on the possibility of studying the measuring capabilities of phonon excitation in surfaces, which directly maps to the study of scattering from insulating surfaces. The fraction of incoherent scattering events for helium scattered off of lithium fluoride has been reported to be less than 10% for 2-keV incident kinetic energy [26]. However, we recall that "coherent" diffraction spots persist in atom-surface grazing scattering off of metallic surfaces, despite the possibility of gapless electronic excitation present in the bulk. More surprisingly, the diffraction spots persist despite an average energy loss. For instance, in He-Ag ⟨110⟩ scattering, Bundaleski *et al.* [10] report diffraction spots despite average scatterer energy losses of 1 eV for scattering at 500 eV, well below the work function threshold; these peaks persist despite blurring at higher energies [27]. Moreover, the energy loss scales superlinearly with incident helium energy. The work by Rubiano *et al.* [28] described the energy loss of the helium atom by viewing it as a frictional loss as the atom scraped against the electron selvage of the surface. A more quantum mechanical description of the helium-surface electronic interaction can be seen via the hybridization potential [29] from the helium atom's occupied electron states and the empty electronic states of the material (from, for instance, the image charges of the helium atom). In the limit of slow atoms, these surface interactions are adiabatic and do not contribute to decoherence or energy transfer. At higher energies, there is the possibility of exciting both these states as well as the gapped empty surface state noted by Goldmann *et al.* [30] which sits ∼1.8 eV above the Fermi level at the surface Brillouin zone k_y edge for Cu⟨110⟩. One can use time-of-flight postselection techniques (as outlined by Busch *et al.* [31]) to look at the helium atoms that have, or have not, excited these surface states. Combining the information provided by classical rainbow diffraction with these energy loss measurements can provide a picture of the surface-scatterer interaction.

Relative to other neutral atomic species, helium is a relatively difficult species to detect as it is light and inert. The above thought experiment, naively stated, requires observing a standing-wave pattern rather than projecting diffracted beams onto a screen, and the corresponding fringe spacing (for shallow incident angle θ) goes as $\hbar\pi\theta^2/\sqrt{8mE}$, which gives subangstrom distances for the parameters given here. While designing the experiment to explicitly test the results presented here is beyond the scope of this work, one possibility for realizing this experimental setup could come via an initial beam split using an initial scattering into low diffraction orders followed by recombination via a Mach-Zehnder interferometer [32]. While for this work we have focused on the regime used by recent helium scattering experiments, there is nothing in the above formalism presented that precludes these ideas from being applied to the previous generation of scattering experiments; the purpose of using the regime chosen here is to limit the possibilities of the types of interactions to vibrational effect and allow the separation of regimes afforded by the slow and fast momenta.

III. SYSTEM EVOLUTION

A. Semiclassical models

Given the difficulty of exactly simulating quantum mechanics, it is necessary to employ approximations in order to obtain meaningful predictions in systems with many degrees of freedoms. Semiclassical methods based on classical mechanics are a natural choice as they can capture quantum behavior while providing an intuitive picture of the system. Moreover, incrementally adding additional quantum features (for instance, different orders of expansions of the semiclassical propagator [33]) to these approximations can provide insight into which effects are indeed quantum mechanical and which are artifacts of classical mechanics.

1. Thawed Gaussians

The thawed Gaussian approximation (TGA), introduced by Heller [34], has been a remarkably successful semiclassical approach to quantum dynamics [35]. Moreover, this technique has been used in time-dependent studies of helium scattering

and was found to have superior convergence properties relative to other semiclassical evolution techniques [36]. The approach is to assume that the wave packet is at all times a Gaussian following a classical guiding central trajectory that is in motion in a perpetual locally quadratic potential. The wave function has the form

$$\Psi(\{\vec{q}\}) = \exp\left[i(\vec{q}-\vec{q}_t)^{\intercal}\underline{\underline{A}}(\vec{q}-\vec{q}_t) + i\vec{p}_{q_t}^{\,\intercal}(\vec{q}-\vec{q}_t) + i\gamma_t\right],$$

which undergoes evolution in the effective Hamiltonian

$$\hat{H}_{\mathrm{TGA}} = \sum_i \frac{p_{q_i}^2}{2m_i} + V(\vec{q}_t) + \sum_i \left.\frac{\partial V}{\partial q_i}\right|_{\vec{q}=\vec{q}_t}(q_i - q_{i_t}) + \frac{1}{2}\sum_{ij}(q_i - q_{i_t})\left.\frac{\partial^2 V}{\partial q_i \partial q_j}\right|_{\vec{q}=\vec{q}_t}(q_j - q_{j_t}).$$

This approximation is reasonable when the second derivative is approximately constant for the width of the wave packet or when the wave packet experiences rapid periodiclike variations that get averaged out over its evolution (a sort of rotating-wave approximation). For the system derived here, we have verified that the thawed Gaussian approximation agrees well in the static case using a reduced-dimensional model evolution of the split-operator fast Fourier transform method (selecting "special angles" so that the particle travels down furrows of an effective one-dimensional potential [37]). We thus expect that it will work well upon inclusion of phonon modes.

2. *Sum of Gaussians plane-wave approach*

Drolshagen and Heller [38] introduced a method to represent a plane wave as a superposition of Gaussian wave packets to model particle-surface scattering and replicate the relative strengths of diffraction peaks in atom-surface scattering measured in experiments. This method captures a greater degree of the wavelike nature of the incident scatterer atoms at the expense of much more expensive computation. We extend this technique using thawed Gaussians for the full system-bath configuration as a means to approach the "standard" way of representing the scattering process in terms incoming and outgoing plane-wave states. We write the initial-state wave function as the superposition

$$\exp(i\vec{k}_0\cdot\vec{r}) \approx \sum_{n_x n_y}^{N_x N_y} \psi_{n_x n_y}^{\mathrm{TGA}}(\vec{r})\exp\left[i\vec{k}_0\cdot\vec{r}_{n_x n_y}\right], \tag{5}$$

where we include $N_x N_y$ wave packets within a single surface unit cell at positions $\vec{r}_{n_x n_y} = \frac{n_x}{N_x}\vec{a}_1 + \frac{n_y}{N_y}\vec{a}_2$ within the unit cell defined by $\vec{a}_1$ and $\vec{a}_2$. We can then evolve all the trajectories together and look at the ground-state overlap $|c_0|$ once again (integrated over the unit cell). It is necessary to wrap trajectories that exit the unit cell back into the unit cell by including the appropriate phase, as well as include trajectories whose wave packet extends into the unit cell of integration.

B. Interaction potential

We describe the nonrelativistic surface scattering problem by considering Schrödinger's equation $\hat{H}\Psi(\vec{r},\vec{q}\,) = i\frac{\partial\Psi}{\partial t}$ with the Hamiltonian

$$\hat{H} = \frac{\vec{p}_r^{\,2}}{2m_s} + \sum_i \frac{\vec{p}_{q_i}^{\,2}}{2m_i} + V(\{\vec{q}_i\}) + V_{\mathrm{int}}(\vec{r},\{\vec{q}_i\}),$$

where $\vec{r}$ refers to the helium particle's coordinates and the $\{\vec{q}_i\}$ denote the surface atom coordinates. We looked at a Cu surface cut at $\langle 110\rangle$ as our model surface. Many different models for the He-Cu interaction potential have been used; for static interactions the corrugated Morse potential has proven quite successful [3]. However, we are interested in modeling the lattice dynamics (and hence the possibility of true elasticity) through the scattering process and so must go to a model that allows us to capture these features.

In order to incorporate the lattice motion and obtain reasonable results compared with static cases, we described the surface-scatterer potential as a pairwise sum of scaled distance exponential potentials, given by

$$V(\vec{r},\{\vec{q}_i\}) = \sum_i v(\vec{r},\vec{q}_i),$$

$$v(\vec{r},\vec{q}_i) = A\,\exp\left[-\beta\sqrt{\sum_\ell \alpha_{(\ell)}\left(r^{(\ell)} - q_i^{(\ell)}\right)^2}\right],$$

where $\ell \in (x,y,z)$. This choice of potential is motivated by the directionality of corrugation as described by Dondi *et al.* [39]; other pairwise atom-surface scattering potentials have been developed (for example, LiF scattering [40,41]). We used parameters found for $E_\perp \approx 240$ meV to be $A = 6$ eV and $\beta = 2.14$ Å^{-1}, and $\alpha_x = 0.6$, $\alpha_y = 1.4$, and $\alpha_z = 1.6$. This matched existing empirical fits by Eichenauer *et al.* [42] and Salanon *et al.* [43] which we verified by comparing potential contours and their relative corrugation and steepness. Finally, we found large overlap of the wave functions evolved in the aforementioned potential versus the trial potential, demonstrating good agreement within the thawed Gaussian approximation.

In order to model the lattice-lattice interaction potential, we treated the Cu$\langle 110\rangle$ lattice as being a harmonic lattice of spherically symmetric atoms with nearest-neighbor interactions with the coupling coefficient $\lambda = 2.28$ eV/Å^2. We use the dynamical matrix approach by Maradudin *et al.* [44] to generate the harmonic lattice potential, giving full periodicity in the surface vectors $\vec{a}_1 = a\hat{x}$ and $\vec{a}_2 = a/\sqrt{2}\hat{y}$ while including the aperiodicity at the surface boundary. This sidesteps dealing with the $\omega = 0$ frequency modes of the lattice and allows us to discover which modes are most excited in the scattering process.

IV. RESULTS

A. Single wave packet

We now examine one set of parameters for the simulation of our thought experiment. We first consider a 100-eV helium particle with an energy spread of ∼1 eV incident upon a Cu$\langle 110\rangle$ surface with a polar angle of $\theta = \pi/64 \approx 2.812^\circ$ and an azimuthal angle of $\phi = 0$ with respect to the $\vec{a}_1$ surface lattice vector. We evolve two separate scattering particle wave packets; the first wave packet ψ_U is sent up toward the surface

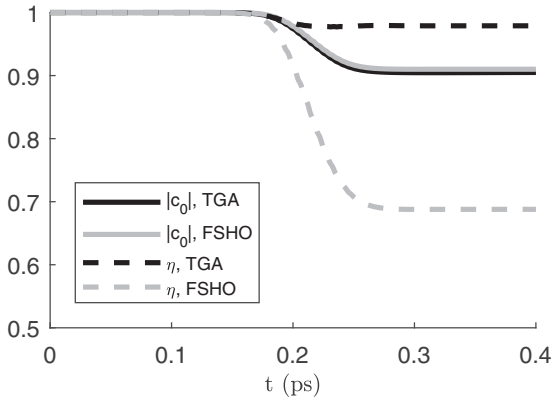

FIG. 3. Lattice ground-state overlap and purity versus time during surface scattering for a thawed Gaussian with $\langle p^2/2m\rangle = 100$ eV, $\theta = 2.8^\circ$, and $\phi = 0$.

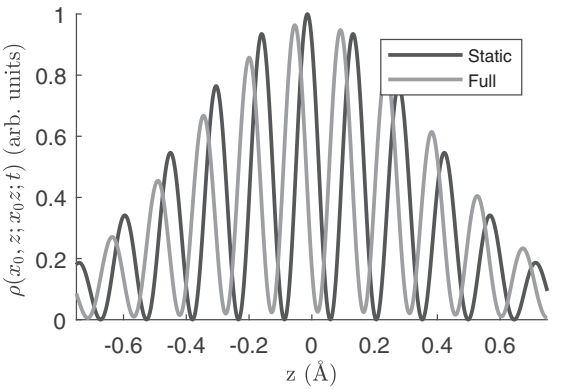

FIG. 4. Slice of the interference pattern of recombined wave packets at the moment of maximal overlap, with $z = 0$ at the center of overlap.

with wave vector $\vec{k} = (\vec{K}, \vec{k}_z)$ to interact with the lattice. The second wave packet ψ_D is sent down with $(\vec{K}, -\vec{k}_z)$ towards a mirror lattice that is held completely static to prevent any interaction. The wave packets are recombined, at which point we may take a snapshot of the reduced total system density matrix to examine the interference fringes. In order to ensure that there are no edge effects in scattering off of the lattice we mirror the lattice points a total of ± 3 times in each direction (in effect, manually inserting the periodic boundary conditions we have established). The lattice is furthermore chosen to be large enough so that by the time the scattering event has finished the particles at the back edge of the slab remain static. We further verified the convergence of our results versus lattice size.

We evolve the semiclassical dynamics using both the forced simple harmonic oscillator (FSHO) model (spiritually equivalent to the frozen Gaussian method [45]) with a plane-wave scatterer and the thawed Gaussian approximation (treating the scatterer and lattice modes together as a wave packet) and look at the resulting dynamics for a $10\times10\times6$ lattice. We plot the ground-state overlap $|c_0|$ and purity $\eta = \mathrm{Tr}[\rho_{\mathrm{red}}^2]$ versus time in Fig. 3.

As we discussed in Sec. II, there is a dramatic difference between evolving a single wave vector versus a wave packet. Both the forced harmonic oscillator and the thawed Gaussian approximation result in rather small degrees of lattice excitation; the final ground-state overlap is slightly lower for the thawed Gaussian case but would produce almost identical degrees of lattice excitation. The thawed Gaussian approximation proves to be a much better method for capturing the self-coherence of the wave packet as the state purity remains high and wavelike throughout the scattering. Note that the diffraction experiments by Schüller *et al.* [9] and Bundaleski *et al.* [10] were performed at higher energies than these parameters; higher-energy scattering excites more phonons and hence have greater degrees of coherence loss.

By looking at a slice in the xz plane at the moment where the outgoing Gaussian wave packets recombine, we can see the instantaneous interference pattern after tracing out the bath. We can compare this to the case where both wave packets interact with completely stationary lattices where the lattice atoms are pinned in place and no excitations are allowed to be generated. We note an ever so slight diminution of interference fringes, shown in Fig. 4. The static-static case yields perfect fringe contrast while the full-static superposition yields a fringe contrast of 0.90, in agreement with our calculations for $|c_0|$ with these parameters. While there is a phase shift between the two traces due to the change in path length from the interaction with the surface, it does not affect the fundamental result.

In a laboratory setting, the particles sent at the surface are more properly treated as plane waves centered around a given energy and momentum rather than a single time-dependent wave packet. We can take the energy-space Fourier transform of the total system-bath wave function $\psi(x, E) = \int e^{iEt}\psi(x, t)dt$, fixing our energy E to reflect this picture. If we again slice along the xz plane, as shown in Fig. 5, we obtain a similar fringe contrast of 0.90 which is consistent with our time-dependent result (i.e., the spread in energy we chose for our thawed Gaussian wave packet does not drastically affect the result).

B. Phonon excitations

We can also look at which lattice modes are excited for a given set of scattering parameters. We can compute the expectation value of the phonon number operator $\langle \hat{n}_i \rangle$ for each lattice mode i from the density matrix of the combined

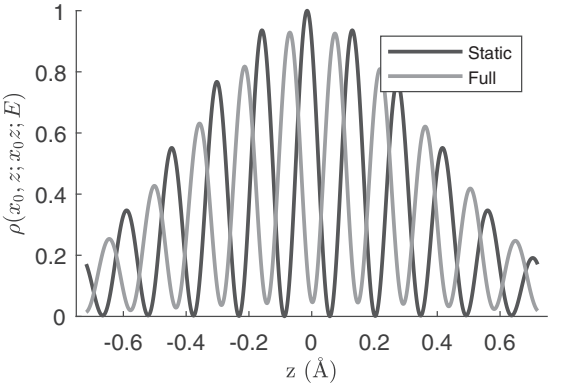

FIG. 5. Slice of the interference pattern of recombined energy-domain transformed wave packets, with $z = 0$ at the center of overlap.

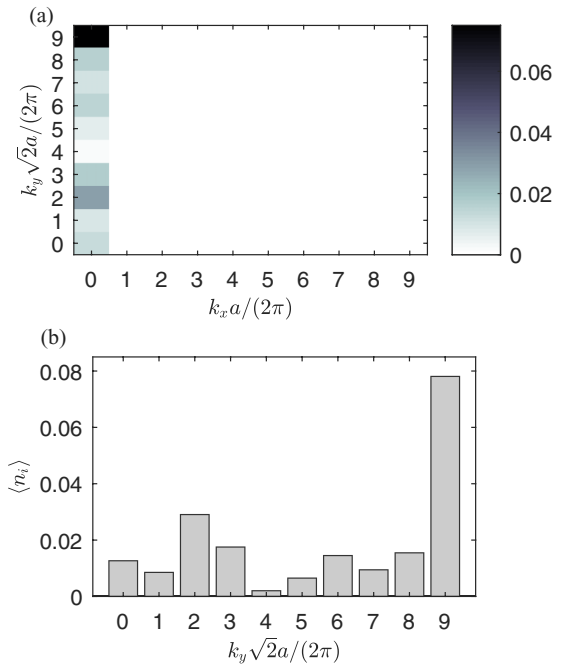

FIG. 6. Individual lattice mode expectation $\langle n_i \rangle$ for (a) all wave vectors and (b) $k_x = 0$.

scatterer-lattice wave function. Then we sum all modes with a given $\vec{k}$ ($3N_z$ modes) and look at the relative contribution of each $\vec{k}$ to the decoherence process, shown in Fig. 6.

While no particular single mode gets heavily excited by the scattering process, it is possibly surprising that the highest excitation occurs for the highest k_y mode (i.e., short-wavelength excitations). This is perhaps more surprising when we consider the classical force vs time that the scatterer experiences, shown in Fig. 7 (note the similarity to the force shown in the work by Roncin and Debiossac [23]): $f_y(t) \approx 0$. Zugarramurdi and Borisov [46] note that for typical experimental fast atom diffraction conditions, there is very little diffraction into reciprocal lattice vectors parallel to the beam direction; this analysis shows very little inelastic scattering in that direction as well.

If we consider the response of the surface atoms to the scatterer as it skitters along the surface, we see that the scatterer experiences a series of "kicks" from each surface atom with a

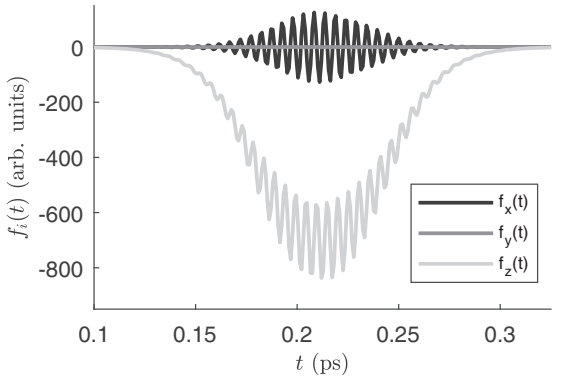

FIG. 7. Force experienced by the scatterer versus time.

broad repulsive background for the z force $f_z(t)$ and a series of spikes for the x force $f_x(t)$ that yield small net x-momentum transfer. Suppose that at a given instant, the scatterer interacts strongly with a particular lattice atom centered at $\vec{r}$. As the scatterer kicks the lattice atom, that lattice atom will then compress the springs connecting it to its nearest-neighbor atoms at $\vec{r} \pm a/2\hat{x} \pm a\sqrt{2}/4\hat{y} + a\sqrt{2}/4\hat{z}$. This causes waves to ripple outward in the $\pm y$ directions of the lattice creating phonons, while the k_x-momentum transfer is negligible due to the rapid attraction-repulsive cycles of the kicks off of the individual atoms in the lattice, parallel to the surface. Aigner *et al.* [47] considered this aspect using a Lindblad master equation formulation with a Monte Carlo ensemble of trajectories to understand the system dynamics and decrease in self-coherence length and observed that the potential parallel to the direction of motion became effectively averaged out; Manson *et al.* [16] described a similar effect in that the fast motion would act as effectively classical dynamics, while the slower motion is more appropriate to describe via quantum dynamics. This effect explains the robustness of our potential model with respect to the parameters we used.

If one looks at the energy distribution of the excited phonon spectra, one can see that the majority of the created phonon quanta emerge from the lowest-energy acoustic modes. The energy deposited into the lattice for the parameters used above (~2.56 meV, which is on the order of the results given by Manson *et al.* [16] for grazing angle collisions) is far smaller than the energy spread in typical helium scattering experiments; as mentioned earlier, the low-energy phonon modes that are excited can be masked by the small total energy change from the lattice nuclear stopping power.

C. Parameter sweeps

We then swept across both parameters to test the robustness of the interference coherence. We found a very weak dependence on the azimuthal angle (with $|c_0|$ varying between 0.86 and 0.91) and found a similarly weak dependence from sweeping the impact factor along the unit cell ($|c_0|$ varying between 0.84 and 0.91). There is a large variance as a consequence of varying the energy; at 400 eV (close to the energy where electronic excitations become important), $|c_0|$ approaches 0.54, while as the incident energy decreases the ground-state overlap increases. Decreasing the polar angle θ while keeping energy fixed also strongly affects the fringe contrast; below 2.8° the fringe contrast approaches 1, however the fringe contrast begins to sharply decrease to $|c_0| = 0.59$ for $\theta = 5°$. We might anticipate this as steeper angles involve fewer, stronger, more localized impacts resulting in the surface more precisely measuring the location of the particle and thus destroying the initially coherent superposition. We can finally adjust the energy and angle together while keeping the momentum perpendicular to the surface fixed at 240 meV; while below $\theta = 2°$ the ground-state overlap reached a fixed asymptote of $|c_0| = 0.96$, above $\theta = 4°$ the ground-state overlap decreases to $|c_0| = 0.60$ for $\theta = 11.2°$, despite a paltry scatterer energy of 6.3 eV.

We also altered the physical parameters of our thought experiment to try to see how different systems might produce more or less decoherence. For realistic lattice constants

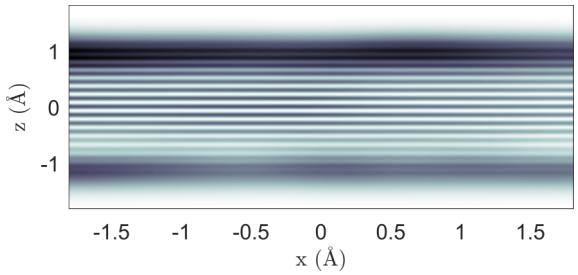

FIG. 8. Recombined interference pattern for the plane wave from the sum of wave packets scattered off of the full lattice, with figure coordinates centered about recombination in z.

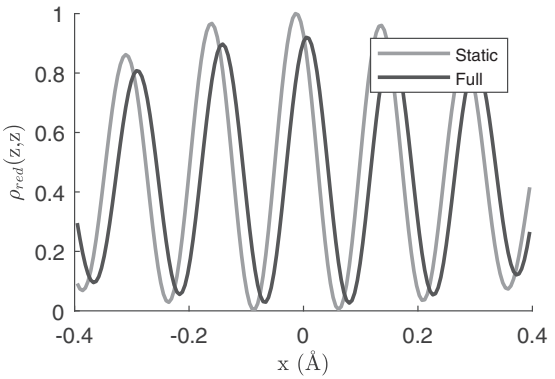

FIG. 9. Slice through the recombined interference pattern from Fig. 8.

between $a = 2.5$ and 5 Å, we saw $|c_0|$ range between 0.86 and 0.93; above $a = 5.5$ Å there was a greater dependence; however, the potential as used here would require further tuning for it to be reasonable. Changing the lattice mass between 20 and 100 amu did not affect the ground-state overlap more than 5%; however, increasing the scatterer mass (keeping energy fixed at 100 eV, hence increasing momentum) produced an approximately linear decrease of $\Delta|c_0| \approx 0.014$ amu^{-1} between 2 and 40 amu. This result was anticipated from the previous discussion [48]. Finally, the results we obtained were very robust to the interaction potential steepness and ranges β and A; there was negligible change in changing β from 0.37 Å^{-1} to 0.67 Å^{-1} and from changing A from 2 eV to 12 eV, implying that the exact details of the potential were not particularly important.

D. Superposition plane wave

We can use the same fundamental approach for our treatment of the plane wave as a sum of wave packets: We can split the incident beam into an interacting component and a noninteracting component to obtain the full initial wave function

$$|\Psi_i\rangle = \frac{1}{\sqrt{2}}(|\psi^{\text{int}}\rangle_{\text{sys}} + |\psi^{\text{non}}\rangle_{\text{sys}})|0\rangle_{\text{bath}}, \tag{6}$$

where the second ket refers to the collective lattice state, taken at $t = 0$ to be in the ground state. We can then obtain the fringe contrast after interaction by computing

$$\int \left| \int \psi^{\text{int}}(\vec{r}, \{q\})\varphi_0^*(\{q\})\, d\vec{q} \right|^2 d\vec{r} = |c_0|^2,$$

where $\varphi_0(\{q\})$ denotes the ground-state lattice wave function. This wave function depicts a time-dependent plane-wave front impinging on the surface.

We used 20×20 wave packets initially assembled in a grid within one unit cell and included a grid of 3×3 neighboring unit cells to avoid edge effects, and computed all quantities by wrapping wave packets (with the appropriate Bloch phase contribution) within a unit cell and numerically integrating over those single unit cells. We found a slightly reduced value for the ground-state overlap $|c_0| \approx 0.89$, which agrees well with the single-wave-packet result and is close to the average of the impact factor results. The time-dependent interference pattern is shown in Fig. 8. There is some blurring in both figures due to the rainbow effect (whose phase contributions yield the Bragg diffraction peaks), but careful examination reveals a slight diminution in the fringe contrast when including the full lattice dynamics.

Taking a slice through the interference pattern [i.e., looking at $\rho_{\text{red}}(\vec{r}, \vec{r})$ from Eq. (4), taking $\vec{r} = (x_0, y_0, z)$ for fixed x_0 and y_0] as shown in Fig. 9 reveals a fringe contrast in the full scatterer plus lattice of 0.89, consistent with the ground-state overlap $|c_0|$ calculated above. We note that there is some reduction in contrast away from the central overlap region of the two beams for both the full and static lattice cases due to the diffracted portions of the beams. The consistency of these results with the single-wave-packet results (both the time- and energy-dependent versions) furthermore indicates that the possibility of diffraction would not affect our primary result.

V. CONCLUSION

The results of this work demonstrate that the existence of diffraction peaks in atom-surface scattering is insufficient to demonstrate whether or not the scattering event was elastic or inelastic. While the existence of truly elastic neutron scattering has been demonstrated in previous works, the radically different nature of atomic scattering (which involves long-range and long-lived interactions with collections of atoms as opposed to the Dirac δ-like interactions characterizing atomic-neutron scattering) has been studied here to examine the possibility of long-wavelength phonon production. Our alternate, interference-pattern-based thought experiment looks to the fundamental quantum notions of the which-way measurement to determine whether these grazing atom-surface scattering events are truly elastic and whether the scattering process acts as a measurement.

[1] G. Boato, P. Cantini, and L. Mattera, Surf. Sci. **55**, 141 (1976).

[2] A. P. Graham, F. Hofmann, J. P. Toennies, and J. R. Manson, J. Chem. Phys. **105**, 2093 (1996).

[3] J. M. Moix, E. Pollak, and W. Allison, J. Chem. Phys. **134**, 024319 (2011).

[4] A. Schüller, S. Wethekam, D. Blauth, H. Winter, F. Aigner, N. Simonović, B. Solleder, J. Burgdörfer, and L. Wirtz, Phys. Rev. A **82**, 062902 (2010).

[5] G. Brusdeylins, R. B. Doak, and J. P. Toennies, Phys. Rev. Lett. **44**, 1417 (1980).

[6] G. Benedek, J. P. Toennies, and R. B. Doak, Phys. Rev. B **28**, 7277 (1983).

[7] M. Petersen, S. Wilke, P. Ruggerone, B. Kohler, and M. Scheffler, Phys. Rev. Lett. **76**, 995 (1996).

[8] P. Rousseau, H. Khemliche, A. G. Borisov, and P. Roncin, Phys. Rev. Lett. **98**, 016104 (2007).

[9] A. Schüller, S. Wethekam, and H. Winter, Phys. Rev. Lett. **98**, 016103 (2007).

[10] N. Bundaleski, H. Khemliche, P. Soulisse, and P. Roncin, Phys. Rev. Lett. **101**, 177601 (2008).

[11] N. Bundaleski, P. Soulisse, A. Momeni, H. Khemliche, and P. Roncin, Nucl. Instrum. Methods Phys. Res. Sect. B **269**, 1216 (2011).

[12] M. Gravielle and J. Miraglia, Nucl. Instrum. Methods Phys. Res. Sect. B **382**, 42 (2016).

[13] J. Seifert, J. Lienemann, A. Schüller, and H. Winter, Nucl. Instrum. Methods Phys. Res. Sect. B **350**, 99 (2015).

[14] R. Feynman, R. Leighton, and M. Sands, *The Feynman Lectures on Physics* (Addison-Wesley, Reading, 1964), Vol. 3.

[15] B. Warren, *X-Ray Diffraction* (Dover, New York, 1990).

[16] J. R. Manson, H. Khemliche, and P. Roncin, Phys. Rev. B **78**, 155408 (2008).

[17] H. Rauch and S. A. Werner, *Neutron Interferometry: Lessons in Experimental Quantum Mechanics* (Clarendon Press, Oxford, 2000).

[18] G. Dolling, H. G. Smith, R. M. Nicklow, P. R. Vijayaraghavan, and M. K. Wilkinson, Phys. Rev. **168**, 970 (1968).

[19] J. Seifert and H. Winter, Phys. Rev. Lett. **108**, 065503 (2012).

[20] G. A. Fiete and E. J. Heller, Phys. Rev. A **68**, 022112 (2003).

[21] M. Born and E. Wolf, *Principles of Optics*, 7th ed. (Cambridge University Press, Cambridge, 1999).

[22] K. Blum, *Density Matrix Theory and Applications* (Plenum, New York, 2010).

[23] P. Roncin and M. Debiossac, Phys. Rev. B **96**, 035415 (2017).

[24] M. Bertino, J. Ellis, F. Hofmann, J. P. Toennies, and J. R. Manson, Phys. Rev. Lett. **73**, 605 (1994).

[25] G. Benedek and J. Toennies, Surf. Sci. **299**, 587 (1994).

[26] J. Lienemann, A. Schüller, D. Blauth, J. Seifert, S. Wethekam, M. Busch, K. Maass, and H. Winter, Phys. Rev. Lett. **106**, 067602 (2011).

[27] M. Busch, A. Schüller, S. Wethekam, and H. Winter, Surf. Sci. **603**, L23 (2009).

[28] C. A. Ríos Rubiano, G. A. Bocan, J. I. Juaristi, and M. S. Gravielle, Phys. Rev. A **89**, 032706 (2014).

[29] J. F. Annett and R. Haydock, Phys. Rev. B **34**, 6860 (1986).

[30] A. Goldmann, V. Dose, and G. Borstel, Phys. Rev. B **32**, 1971 (1985).

[31] M. Busch, J. Lienemann, J. Seifert, A. Schüller, and H. Winter, Vacuum **86**, 1618 (2012).

[32] R. Delhuille, C. Champenois, M. Büchner, L. Jozefowski, C. Rizzo, G. Trénec, and J. Vigué, Appl. Phys. B **74**, 489 (2002).

[33] L. Kocia and E. J. Heller, J. Chem. Phys. **141**, 181102 (2014).

[34] E. J. Heller, J. Chem. Phys. **62**, 1544 (1975).

[35] E. J. Heller, Acc. Chem. Res. **39**, 127 (2006).

[36] J. M. Moix and E. Pollak, Phys. Rev. A **79**, 062507 (2009).

[37] A. Ruiz, J. P. Palao, and E. J. Heller, Phys. Rev. A **79**, 052901 (2009).

[38] G. Drolshagen and E. J. Heller, J. Chem. Phys. **79**, 2072 (1983).

[39] M. G. Dondi, S. Terreni, F. Tommasini, and U. Linke, Phys. Rev. B **37**, 8034 (1988).

[40] V. Celli, D. Eichenauer, A. Kaufhold, and J. P. Toennies, J. Chem. Phys. **83**, 2504 (1985).

[41] J. E. Miraglia and M. S. Gravielle, Phys. Rev. A **95**, 022710 (2017).

[42] D. Eichenauer, U. Harten, J. P. Toennies, and V. Celli, J. Chem. Phys. **86**, 3693 (1987).

[43] B. Salanon, G. Armand, J. Perreau, and J. Lapujoulade, Surf. Sci. **127**, 135 (1983).

[44] A. Maradudin, E. Montroll, G. Weiss, and I. Ipatova, *Theory of Lattice Dynamics in the Harmonic Approximation*, 2nd ed. (Academic Press, New York, 1971).

[45] E. J. Heller, J. Chem. Phys. **75**, 2923 (1981).

[46] A. Zugarramurdi and A. G. Borisov, Phys. Rev. A **86**, 062903 (2012).

[47] F. Aigner, N. Simonović, B. Solleder, L. Wirtz, and J. Burgdörfer, Phys. Rev. Lett. **101**, 253201 (2008).

[48] H. Khemliche, N. Bundaleski, P. Soulisse, and P. Roncin, Nucl. Instrum. Methods Phys. Res. Sect. B **267**, 620 (2009).